IIETA International Information and Engineering Technology Association
Advancing the World of Information and Engineering

Mathematical Modelling of Engineering Problems
Vol. 9, No. 5, October, 2022, pp. 1359-1368
Journal homepage: http://iieta.org/journals/mmep

Analytical Procedure for the Flow of a Carreau-Yasuda Fluid Through the Diseased Tapered Inclined Artery Subject to Heat Transfer and Chemical Reactions

Mahmoud Abdallah El Kot[1,2]

[1] Department of Mathematics, College of Sciences and Arts, Dhahran Aljanoub, King Khalid University, Abha 61421, Saudi Arabia
[2] Department of Mathematics and Computer Science, Faculty of Science, Suez University, Suez 43533, Egypt

Corresponding Author Email: melkot@kku.edu.sa

https://doi.org/10.18280/mmep.090526

Received: 3 June 2022
Accepted: 19 October 2022

Keywords:
blood flow, Carreau-Yasuda fluid, diseased artery, heat transfer, chemical reactions

ABSTRACT

This paper demonstrates the implications of heat transfer and chemical reactions by considering the flow of a Carreau-Yasuda fluid through the diseased tapered inclined artery. The analysis has performed on the artery with mild stenosis. The analytical solution has been obtained using the perturbation method due to its low Weissenberg number to get the blood velocity, the wall shear stress distribution, the temperature, the concentration, the resistance impedance and the stream function. The critical results in this study have depicted that the blood velocity for dilatant fluid is higher than that in viscous and pseudoplastic fluids in the core region of the artery. The value of blood velocity through a Newtonian fluid is extraordinarily lower than that through a Carreau-Yasuda fluid at the core region of the artery. The magnitude of blood velocity across the vertical artery is higher than those in the inclined and horizontal arteries inside the core region of the artery. The wall shear stress distributions are higher in the case of stenosis (diseased artery) than in no stenosis (healthy artery). The temperature transmission for the Carreau fluid is higher than that for the Carreau-Yasuda fluid. The flow resistance progressively increases as the depth of the stenosis increases. The size of the trapping bolus gradually increases, shifting toward the right at the diverging tapering artery, and it gradually increases, moving toward the left at the converging tapering artery. Finally, the streamlines are noticeably more comprehensive along the vertical artery and are higher than those in the inclined and horizontal arteries.

1. INTRODUCTION

Arterial stenosis is a lumen narrowing that harasses blood flow to blood vessels. Vascular stenosis may be caused by aneurysms and tumours or linked to arteriosclerosis. Arterial stenosis has motivated biomechanics scientists to execute blood flow awareness and empirical measurement of pressure and velocity in human organs [1].

The Carreau-Yasuda fluid is a known rheological model utilized to appreciate the steady-state viscosity in non-Newtonian fluid (e.g. pendants, emulsions, and polymer solvents). Non-Newtonian Carreau-Yasuda fluid is the generalized form of Carreau fluid and has numerous industrial implementations like food treatment, drilling, bio-engineering processes etc. [2]. Carreau-Yasuda fluid model predicts the shear-thinning/shear-thickening behaviours, which display diverse impacts on the thermal-transfer features of fluid [3]. Although various circumstances may appear in these fluids, they have displayed shear-thinning behaviour; this refers to the viscosity dwindling due to a plus in the malformation rate implemented to the fluid [4]. The Carreau-Yasuda model has received widespread emphasis due to its nature being most suitable for depicting shear-thinning fluid [5]. A few research attempts to study Carreau-Yasuda fluid flow through narrowed arteries under certain physical conditions, but it lacks the analytical mathematical procedure [6-10].

The contemplation of the impacts of heat and chemical reactions on blood flow is impressive to many researchers. Heat and mass transfer survey is the needful theme for researchers due to their biomedical engineering utilizations like tissue delivery and food treatment. So, the effect of rheological features of the fluid with a synchronized scattering of heat and mass transfer is located in enormous indication [11]. The quantitative anticipation of blood flow rate and heat build-up is pivotal for personifying blood circulation disease and gauging blood glucose [12].

Motivated by the studies mentioned above, the unsteady flow of Carreau-Yasuda fluid across the oblique stenosed catheterized artery in the presence of heat transfer and chemical reactions are considered in this paper. The problem has been modelled, and then the non-dimensional governing equations for mild stenosis with the corresponding boundary conditions have been depicted and solved analytically utilizing the perturbation technique. Graphical results and discussions are explained, and some conclusions are included.

2. PROBLEM FORMULATION

An inclined arterial segment with overlapping stenosis can be modelled as a superfine solid cylindrical of finite length L. The non-Newtonian incompressible Carreau-Yasuda fluid (as a blood model) is injected into the arterial segment. The cylindrical polar coordinate (r, θ, z) is chosen where the z-axis

is picked along the arterial segment axis, and all flow parameters are independent of the direction θ. Moreover,, asuming that r=0 is selected as the axis of the symmetry of the arterial segment. The heat and mass transfer phenomena are subjected by afforcing heat T_0 and concentration C_0 to the artery's wall, while at the centre of the artery, we are considering symmetry conditions on both temperature and concentration. The geometrical shape of the constricted inclined tapered artery is chosen (see Figure 1) [13].

$$R(z)=\begin{cases} h(z)\left(1-\dfrac{\delta\cos\phi(z-d)}{R_oL_o}\left\{11-\dfrac{94(z-d)}{3L_o}+\dfrac{32(z-d)^2}{L_o^2}-\dfrac{32(z-d)^3}{3L_o^3}\right\}\right) & d\le z\le d+\dfrac{3L_o}{2} \\ h(z) & \text{otherwise} \end{cases} \tag{1}$$

with

$$h(z)=mz+R_o \tag{2}$$

where, $h(z)$ is the radius of the tapering arterial segment in the narrowed region, R_0 is the radius of the non-tapering artery in the non-narrowed region, m=tanφ symbolize the slope of the tapering vessel, φ is the angle of tapering where the possibility of diverse forms of the artery viz, the converging tapering (φ<0), non-tapered artery (φ=0) and the diverging tapering (φ>0) [14]. $3L_0/2$ is the extent of overlapping stenosis, d is the site of the narrowing. Here, δ is the maximum altitude of the stenosis, such that the ratio δ/R_0<<1, appears at two specific locations, i.e., $z=d+L_0/2$ and $z=d+L_0$. The height of the stenosis at a distance of $z=d+3L_0/4$ from the origin is $3\delta/4$ and $\delta\cos\varphi$ is taken to be the maximum altitude of overlapping stenosis.

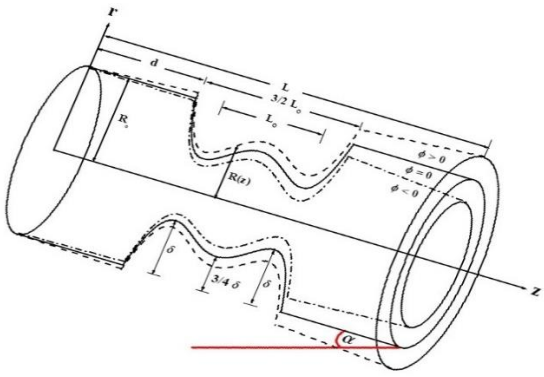

Figure 1. Graphical scheme of inclined tapered overlapping narrowed artery

The following governing equations may list the mathematical description of the problem:

Continuity:

$$\frac{\partial V_r}{\partial r}+\frac{V_r}{r}+\frac{\partial V_z}{\partial z}=0 \tag{3}$$

Momentum:

$$\rho\left(\frac{\partial V_r}{\partial t}+V_r\frac{\partial V_r}{\partial r}+V_z\frac{\partial V_r}{\partial z}\right) =-\frac{\partial p}{\partial r}+\frac{1}{r}\frac{\partial}{\partial r}(rS_{rr})+\frac{\partial S_{rz}}{\partial z}-\frac{S_{\theta\theta}}{r}-\rho g\cos\alpha \tag{4}$$

$$\rho\left(\frac{\partial V_z}{\partial t}+V_r\frac{\partial V_z}{\partial r}+V_z\frac{\partial V_z}{\partial z}\right) =-\frac{\partial p}{\partial z}+\frac{1}{r}\frac{\partial}{\partial r}(rS_{rz})+\frac{\partial S_{zz}}{\partial z}+\rho g\sin\alpha \tag{5}$$

Energy equation:

$$\rho c_p\left(\frac{\partial T}{\partial t}+V_r\frac{\partial T}{\partial r}+V_z\frac{\partial T}{\partial z}\right)=S_{rr}\frac{\partial V_r}{\partial r}+S_{rz}\frac{\partial V_z}{\partial r} +S_{zr}\frac{\partial V_r}{\partial z}+S_{zz}\frac{\partial V_z}{\partial z}+K\left(\frac{\partial^2T}{\partial r^2}+\frac{1}{r}\frac{\partial T}{\partial r}+\frac{\partial^2T}{\partial z^2}\right) \tag{6}$$

Concentration equation:

$$\frac{\partial C}{\partial t}+V_r\frac{\partial C}{\partial r}+V_z\frac{\partial C}{\partial z}=D\left(\frac{\partial^2C}{\partial r^2}+\frac{1}{r}\frac{\partial C}{\partial r}+\frac{\partial^2C}{\partial z^2}\right) +\frac{DK_T}{T_m}\left(\frac{\partial^2T}{\partial r^2}+\frac{1}{r}\frac{\partial T}{\partial r}+\frac{\partial^2T}{\partial z^2}\right) \tag{7}$$

where, p represents the pressure of the fluid, ρ is the density of the fluid, V_r and V_z are the components of the velocity in radial and axial directions respectively, g represent gravitational acceleration, α is tilt angle, T is the temperature, c_p is the specific heat at fixed pressure, K denotes the thermal conductivity, C is the concentration of fluid, D is diffusion coefficient, K_T is the thermal-diffusion ratio, and T_m is the temperature of the medium. The supplementary stress tensor for Carreau-Yasuda fluid is identificated by [2, 3, 15-21]:

$$S=\mu_o\left[\frac{\mu_\infty}{\mu_o}+\left(1-\frac{\mu_\infty}{\mu_o}\right)\left(1+(\Gamma\dot\gamma)^q\right)^{\frac{n-1}{q}}\right]A_1 \tag{8}$$

with

$$A_1=\nabla V+(\nabla V)^T,\ \dot\gamma=\sqrt{\frac{1}{2}tr(A_1)^2} \tag{9}$$

where, μ_∞ is viscosity at infinite shear rate, μ_0 is viscosity at zero shear rate, Γ is time constant, $\dot\gamma$ is shear rate, q is Carreau-Yasuda parameter, n is power low index number, A_1 is first Rivlin Ericksen tensor and V=(V_r, 0, V_z) is velocity vector.

Assume μ_∞/μ_0 to be very small. Eq. (8) becomes

$$S=\mu_o\left[\left(1+(\Gamma\dot\gamma)^q\right)^{\frac{n-1}{q}}\right]A_1 \tag{10}$$

and for the case $\Gamma\dot\gamma$<<1, Eq. (10) is reduced to

$$S=\mu_o\left[1+\frac{n-1}{q}(\Gamma\dot\gamma)^q\right]A_1 \tag{11}$$

The specified status of viscous fluid is kept at (n=1). Also, there are two various issues i.e., (n>1) leads to the dilatant

fluid and (n<1) drives to pseudoplastic fluid. The original Carreau fluid model can also be retained by substituting (q=2).

The boundary conditions are:

$$V_r = 0,\ \frac{\partial V_z}{\partial r} = 0,\ \frac{\partial T}{\partial r} = 0,\ \frac{\partial C}{\partial r} = 0 \ \text{ on } \ r = 0 \tag{12}$$

$$V_r = 0,\ V_z = 0,\ T = T_o,\ C = C_o \ \text{ on } \ r = R \tag{13}$$

Using the following dimensionless variables:

$$\begin{aligned}
&r = R_o r',\ z = L_o z',\ V_r = \frac{\delta u_o}{L_o} V_r',\ V_z = u_o V_z',\\
&R = R_o R',\ t = \frac{L_o}{u_o} t',\ p = \frac{u_o L_o \mu_o}{R_o^2} p', \theta = \frac{T - T_o}{T_o},\\
&\sigma = \frac{C - C_o}{C_o},\ S_{rr} = \frac{u_o \mu_o}{L_o} S_{rr}', S_{rz} = \frac{\mu_o u_o}{R_o} S_{rz}',\\
&S_{zr} = \frac{\mu_o u_o}{R_o} S_{zr}', S_{zz} = \frac{\mu_o u_o}{L_o} S_{zz}',\ S_{\theta\theta} = \frac{\mu_o u_o}{L_o} S_{\theta\theta}',\\
&\dot{\gamma} = \frac{u_o}{R_o}\dot{\gamma}', R_e = \frac{\rho u_o R_o}{\mu_o}, F_r = \frac{u_o^2}{g R_o},\ P_r = \frac{c_p \mu_o}{K},\\
&B_r = \frac{\mu_o u_o^2}{K T_o},\ S_c = \frac{\mu_o}{\rho D},\ S_r = \frac{\rho D K_T T_o}{\mu_o T_m C_o}, W_e = \frac{\Gamma u_o}{R_o},
\end{aligned} \tag{14}$$

where, u_0 is the average velocity of the fluid over arterial segment, R_e is Reynolds number, F_r is the Froud number, P_r is Prandtl number, B_r is Brickmann number, S_c is Schmidt number and S_r is Soret number, W_e is Weissenberg number. Let us facilitate the governing equations for mild stenosis by adoptiving the two conditions $\left(\delta^* = \frac{\delta}{R_o} << 1\right)$ and $\left(\varepsilon = \frac{R_o}{L_o} \sim o(1)\right)$ [22].

$$\frac{\partial V_z}{\partial z} = 0 \tag{15}$$

$$\frac{\partial p}{\partial r} = 0 \tag{16}$$

$$\frac{\partial p}{\partial z} = \frac{1}{r}\frac{\partial}{\partial r}\left(r\left\{\left(\frac{\partial V_z}{\partial r}\right) + \frac{n-1}{q}(W_e)^q \left(\frac{\partial V_z}{\partial r}\right)^{q+1}\right\}\right) + \frac{R_e \sin\alpha}{F_r} \tag{17}$$

$$\frac{1}{r}\frac{\partial}{\partial r}\left(r\frac{\partial \theta}{\partial r}\right) = -B_r\left(\left(\frac{\partial V_z}{\partial r}\right)^2 + \frac{n-1}{q}(W_e)^q \left(\frac{\partial V_z}{\partial r}\right)^{q+2}\right) \tag{18}$$

$$\frac{1}{r}\frac{\partial}{\partial r}\left(r\frac{\partial \sigma}{\partial r}\right) = -S_r S_c \frac{1}{r}\frac{\partial}{\partial r}\left(r\frac{\partial \theta}{\partial r}\right) \tag{19}$$

The corresponding boundary conditions (dropping dashes):

$$\frac{\partial V_z}{\partial r} = 0\ ,\ \frac{\partial \theta}{\partial r} = 0\ ,\ \frac{\partial \sigma}{\partial r} = 0 \ \text{ on } \ r = 0 \tag{20}$$

$$V_z = 0\ ,\ \theta = 0\ ,\ \sigma = 0 \ \text{ on } \ r = R \tag{21}$$

$$R(z) = \begin{cases} h^*(z)\left(1 - \delta^* \cos\phi\left(z - d^*\right)\left\{11 - \dfrac{94\left(z-d^*\right)}{3} + 32\left(z-d^*\right)^2 - \dfrac{32\left(z-d^*\right)^3}{3}\right\}\right) & d^* \le z \le d^* + \dfrac{3}{2} \\ h^*(z) & \text{otherwise} \end{cases} \tag{22}$$

where, $h^*(z)=m^*z+1$, $d^*=d/L_0$ and $m^*= L_0m/R_0$ is the corresponding slope of the tapered vessel.

3. SOLUTION DEVELOPMENT

We extend the dependent variables as:

$$\begin{aligned}
V_z &= V_{zo} + (W_e)^q V_{z1} + O(W_e)^{2q}\\
\frac{dp}{dz} &= \frac{dp_o}{dz} + (W_e)^q \frac{dp_1}{dz} + O(W_e)^{2q}\\
F &= F_o + (W_e)^q F_1 + O(W_e)^{2q}\\
\theta &= \theta_o + (W_e)^q \theta_1 + O(W_e)^{2q}\\
\sigma &= \sigma_o + (W_e)^q \sigma_1 + O(W_e)^{2q}
\end{aligned} \tag{23}$$

The solutions of pressure gradient, axial velocity, temperature and concentration with the corresponding boundary conditions are

$$\frac{dp}{dz} = -\frac{16F}{R^4} + \frac{R_e \sin\alpha}{F_r} + \frac{(W_e)^q (n-1)}{2^{q-2} q(q+4)} \times \left(\frac{dp_o}{dz} - \frac{R_e \sin\alpha}{F_r}\right)^{q+1} R^q \tag{24}$$

$$V_z = \frac{1}{4}\left(\frac{dp}{dz} - \frac{R_e \sin\alpha}{F_r}\right)\left(r^2 - R^2\right) - \frac{(W_e)^q (n-1)}{2^{q+1} q(q+2)}\left(\frac{dp_o}{dz} - \frac{R_e \sin\alpha}{F_r}\right)^{q+1} \times \left(r^{q+2} - R^{q+2}\right) \tag{25}$$

$$\theta = -2B_r\left(\frac{dp_o}{dz} - \frac{R_e \sin\alpha}{F_r}\right) \times \left[\frac{1}{64}\left(\frac{dp}{dz} - \frac{1}{2}\left(\frac{dp_o}{dz} + \frac{R_e \sin\alpha}{F_r}\right)\right)\left(r^4 - R^4\right) - \frac{(W_e)^q (n-1)}{2^{q+3} q(q+4)^2}\left(\frac{dp_o}{dz} - \frac{R_e \sin\alpha}{F_r}\right)^{q+1} \times \left(r^{q+4} - R^{q+4}\right)\right] \tag{26}$$

$$\sigma = 2B_r S_r S_c \left(\frac{dp_o}{dz} - \frac{R_e \sin\alpha}{F_r}\right) \times \left[\frac{1}{64}\left(\frac{dp}{dz} - \frac{1}{2}\left(\frac{dp_o}{dz} + \frac{R_e \sin\alpha}{F_r}\right)\right)\left(r^4 - R^4\right) - \frac{(W_e)^q (n-1)}{2^{q+3} q (q+4)^2}\left(\frac{dp_o}{dz} - \frac{R_e \sin\alpha}{F_r}\right)^{q+1} \times \left(r^{q+4} - R^{q+4}\right)\right] \quad (27)$$

Using Eq. (25), the wall shear stress can be listed as

$$\tau_R = \frac{1}{2}\left(\frac{dp}{dz} - \frac{R_e \sin\alpha}{F_r}\right) R - \frac{(W_e)^q (n-1)}{2^{q+1} q} \times \left(\frac{dp_o}{dz} - \frac{R_e \sin\alpha}{F_r}\right)^{q+1} R^{q+1} \quad (28)$$

The stream function $\left(V_z = \frac{1}{r}\frac{\partial \psi}{\partial r} \text{ with } \psi = 0 \text{ at } r = 0\right)$ is

$$\psi = \frac{1}{4}\left(\frac{dp}{dz} - \frac{R_e \sin\alpha}{F_r}\right)\left(\frac{r^4}{4} - \frac{r^2 R^2}{2}\right) - \frac{(W_e)^q (n-1)}{2^{q+1} q (q+2)}\left(\frac{dp_o}{dz} - \frac{R_e \sin\alpha}{F_r}\right)^{q+1} \times \left(\frac{r^{q+4}}{q+4} - \frac{r^2 R^{q+2}}{2}\right) \quad (29)$$

Assuming the flow rate is fixed for all the syllables of artery. The pressure drop along the overlapping stenosis is

$$\Delta p = \int_0^{L^*} \left(-\frac{dp}{dz}\right) dz = F \int_0^{L^*} \chi(z)\, dz \quad (30)$$

where,

$$\chi(z) = \frac{16}{R^4} - \frac{R_e \sin\alpha}{F F_r} - \frac{(W_e)^q (n-1)}{2^{q-2} q (q+4) F} \times \left(\frac{dp_o}{dz} - \frac{R_e \sin\alpha}{F_r}\right)^{q+1} R^q \quad (31)$$

The resistance impedance exposed by the flowing blood in the arterial segment under deem using Eq. (30) may be recognised as

$$\lambda = \frac{\Delta p}{F} = \int_0^{d^*} \Sigma(z)\, dz + \int_{d^*}^{d^*+\frac{3}{2}} \chi(z)\, dz + \int_{d^*+\frac{3}{2}}^{L^*} \Sigma(z)\, dz \quad (32)$$

where, $L^*=L/L_0$ and $\sum(z)=\chi(z)|_{m*z+1}$.

4. DISCUSSION OF NUMERICAL RESULTS

This paper uses computer simulations of blood flow in diseased tapered inclined arteries subject to heat transfer and chemical reactions. In this part, we exhibit drawing illustrations of some essential features of the flow features, like blood velocity, wall shear stress, temperature, concentration, resistance impedance and the trapping phenomenon for distinct values of power low index parameter n, Weissenberg parameter W_e, tilt angle α, Froud parameter F_r, angle of tapering φ, maximum constriction altitude δ^*, the Brickmann parameter B_r, the Soret parameter S_r and the length of the artery L. For the goal of numerical calculations, we use the following informations (R_e=1, dp_0/dz=-0015, F=0.3, d^*=0.75). The numerical results are simulated in the following figures below to get a deeper insight into the qualitative analysis of the results.

The impacts of power low index number n and Weissenberg parameter W_e on the velocity profile of blood are analyzed. Figure 2(a) describes how the blood velocity varies with power low index number. The blood velocity declines with an increment in the exponent number in the two terminal regions and whilst the blood velocity increases with a rise in the exponent number in the core region. Moreover, the curves of dilatant fluid (n>1) are higher than those in the viscous fluid (n=1) and the pseudoplastic fluid (n<1) in the core region. Figure 2(b) shows the behaviour of the axial velocity with the Weissenberg parameter W_e. The velocity increases as the Weissenberg parameter increases in the core region this consistent with the results of Khan et al. [2]. At the same time, the opposite happens in the two terminal regions. Furthermore, the values of blood velocity for a Newtonian fluid (W_e=0 or n=1) are lower than that for a Carreau-Yasuda fluid (W_e≠0 or n≠1) at the core region. The archaeology of tilt angle α and Froud parameter F_r on blood velocity V_z are presented in Figures 3(a) and 3(b). The magnitude of the blood velocity across the vertical artery (α=90°) is superior than those across inclined artery (α=30°) and horizontal artery (α=0°) inside the core region, while the inverse occurs at the two terminal ends.

We can also record that blood velocity grows by a rise in the Froud number F_r near the two terminal ends. At the same time, it reduces by dwindling the Froud number F_r at the core region.

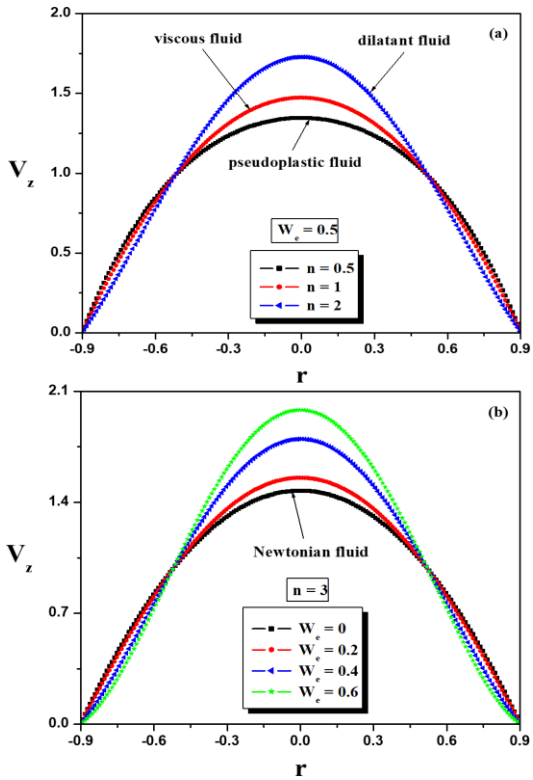

Figure 2. Variance of velocity aspects V_z versus r for diversified values of n and W_e at z=1.2, δ^*=0.09, φ=0, q=3, α=15°, F_r=0.1 (panels (a) and (b) respectively)

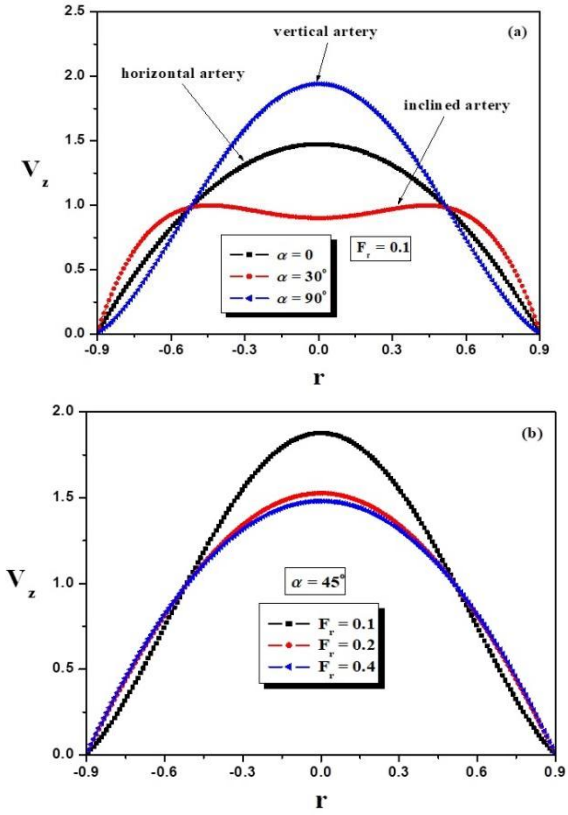

Figure 3. Variance of velocity aspects V_z versus r for diversified values of α and F_r at z=1.2, δ^*=0.09, φ=0, W_e=0.3, q=2, n=3 (panels (a) and (b) respectively)

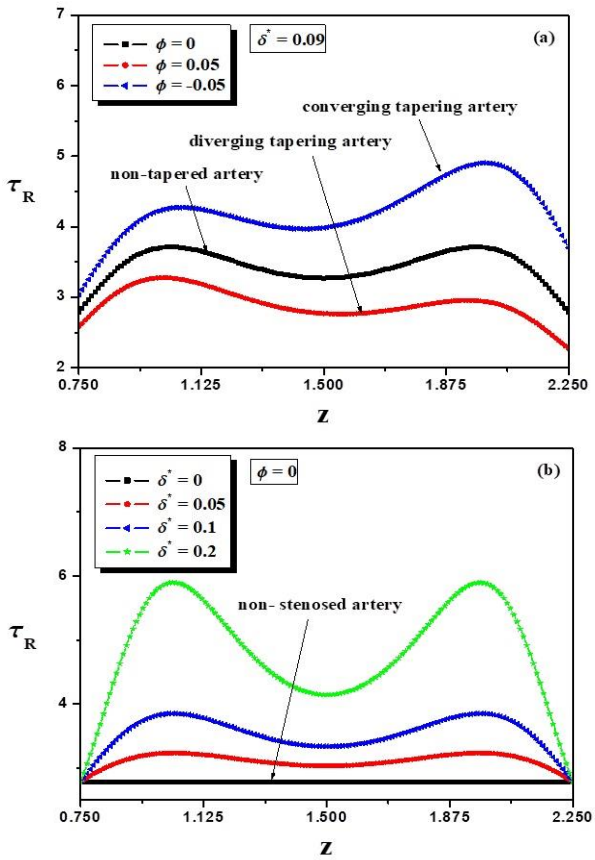

Figure 4. Distribution of wall shear stress τ_R versus z for diverse values of φ and δ^* at W_e=0.1, q=2, n=3, α=30°, F_r=0.1 (panels (a) and (b) respectively)

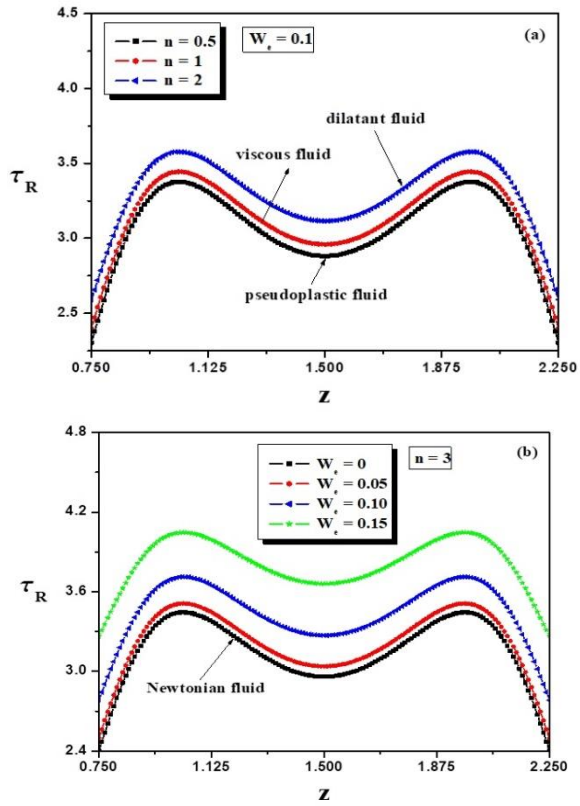

Figure 5. Distribution of wall shear stress τ_R versus z for diverse values of n and W_e at δ^*=0.09, φ=0, q=2, α=30°, F_r=0.1 (panels (a) and (b) respectively)

The profiles of wall shear stress τ_R in the narrow area ($0.75 \le z \le 2.25$) for distinct values of taper angle φ, and maximum constriction altitude δ^* are displayed in Figures 4(a) and 4(b), consecutively. Figure 4(a) indicates that the curves via the converging tapering artery (φ=-0.05<0) are above those in the non-tapering artery (φ=0) and the diverging tapering artery (φ=0.05>0). This is consistent with the results of Padma et al. [23]. Figure 4(b) depicts that the wall shear stress increases from the purely healthy artery (no stenosis) to the diseased artery case because the augmentation of the maximum constriction altitude decelerates the flow and increases wall stress. Hence, the wall shear stress disturbances are higher for stenosis ($\delta^* \neq 0$) (diseased artery) than that for no stenosis (δ^*=0) (healthy artery). The wall shear stress distros along the narrow zone for diversified values of the power low index parameter n and the Weissenberg number W_e are exhibited in Figures 5(a) and 5(b). It should be observed that the shear wall stress increases as the values of n and W_e increase. It is surprisingly enjoyable to note that the exponent number n has a reinforcing impact on the wall shear stress. The consequences in Figure 5(a) show that the curves of wall shear stress for dilatant fluid (n>1) are higher than those in the viscous fluid (n=1) and the pseudoplastic fluid (n<1). It also reveals that from Figure 5(b), the values of wall shear stress for Carreau-Yasuda fluid ($W_e \neq 0$) are substantially maximal than that for Newtonian fluid (W_e=0). The results of wall shear stress distributed over arterial segment for diversified values of the angle of inclination α and Froud number F_r are presented in Figures 6(a) and 6(b). It might be evident that the shear stress distribution along the inclined vessel (α=30°) is superior to those in the horizontal vessel (α=0°) and the vertical vessel (α=90°). Also, the wall shear stress increases by growing the Froud number F_r.

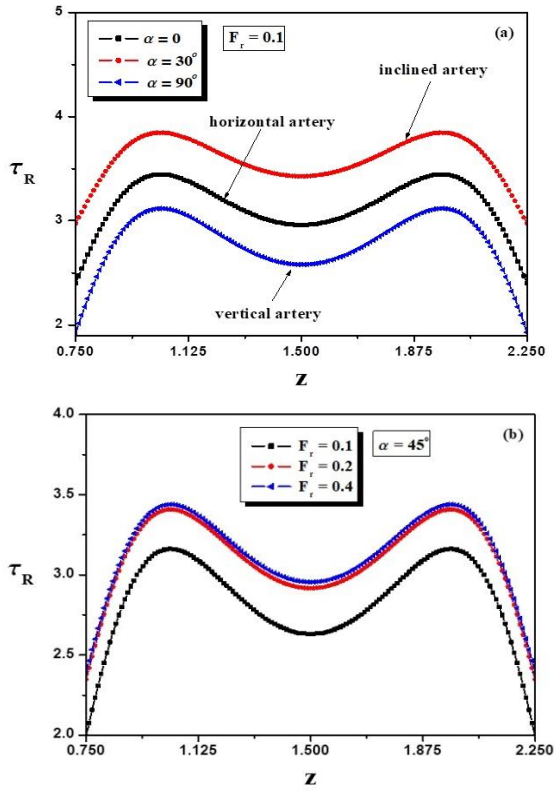

Figure 6. Distribution of wall shear stress τ_R versus z for diverse values of α and F_r at δ^*=0.09, φ=0, W_e=0.1, q=2, n=4 (panels (a) and (b) respectively)

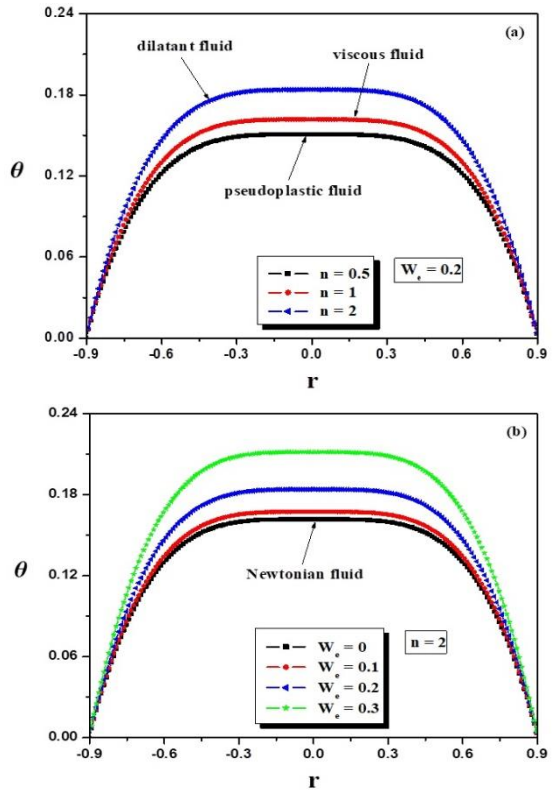

Figure 7. Variation of tempresure θ versus r for diverse values of n and W_e at z=1.2, δ^*=0.09, φ=0, q=2, α=15°, F_r=0.1, B_r=0.3 (panels (a) and (b) respectively)

The variation of temperature θ with radial distance r presented in Figures 7(a) and 7(b) predict the effects of the exponent number n and the Weissenberg parameter W_e on the thermal transmission of the fluid while Figures 8(a) and 8(b) help making a comparative study of the mass transfer for various values of the Carreau-Yasuda parameter q and the Brickmann number B_r. All these results suggest that the non-dimensional temperature of the fluid increases with the increase of the power low index number n, Weissenberg number W_e, and the Brickmann number B_r while it decreases by increasing of the Carreau-Yasuda parameter q. Figure 7(a) depicts that the dimensionless heat transfer rate for the dilatant fluid (n>1) is maximal than that in the viscous fluid (n=1) and the pseudoplastic fluid (n<1). It is observed that the heat values for a Newtonian fluid (W_e=0) are much less than that for the Carreau-Yasuda fluid (W_e≠0), as shown in 7(b). Moreover, the transmission of the temperature for Carreau fluid (q=2) is higher than that for Carreau-Yasuda fluid (q≠2), as described in Figure 8(a). It can be seen in Figure 8(b) that, the higher Brickmann number value, the larger temperature of the fluid rise. This is consistent with the results of Nazir et al. [11] and Farooq et al. [24].

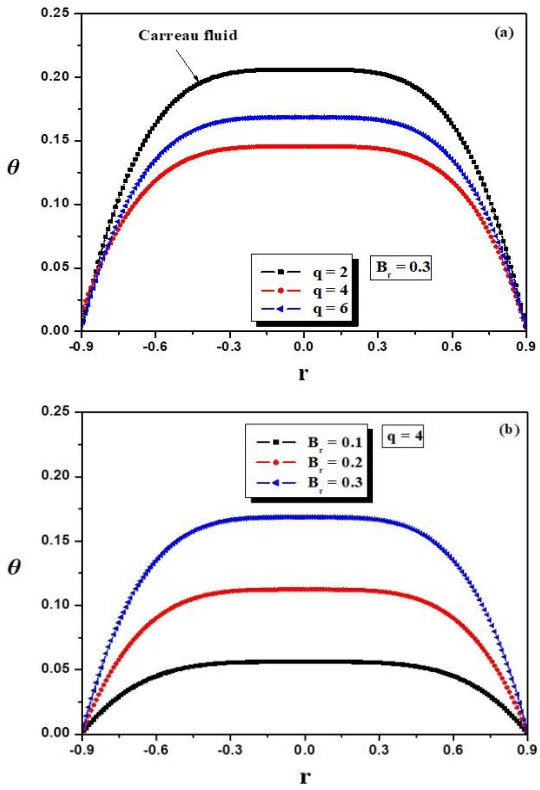

Figure 8. Variation of tempresure θ versus r for diverse values of q and B_r at z=1.2, δ^*=0.09, φ=0, W_e=0.2, α=15°, n=3, F_r=0.1 (panels (a) and (b) respectively)

Figures 9 and 10 are intended to show the disparity of concentration for the power low index parameter n, the Weissenberg number W_e, the Brickmann number B_r, and the Soret parameter S_r. It is observed that the concentration has an adverse behaviour as compared to the temperature. Figures 9(a) and 9(b) depict that the concentration for the dilatant liquid (n>1) is more minimal than that for the viscous liquid (n=1) and the pseudoplastic liquid (n<1). Also, the concentration for a Newtonian fluid (W_e=0) is maximal than that for Carreau-Yasuda fluid (W_e≠0). Figures 10(b) and 10(b) explain the difference of concentration profile for the Brickmann parameter B_r, and the Soret parameter S_r to show

the concentration of the fluid decreases as the Brickmann parameter B_r and the Soret parameter S_r increase. This is consistent with the results of Alam et al. [25].

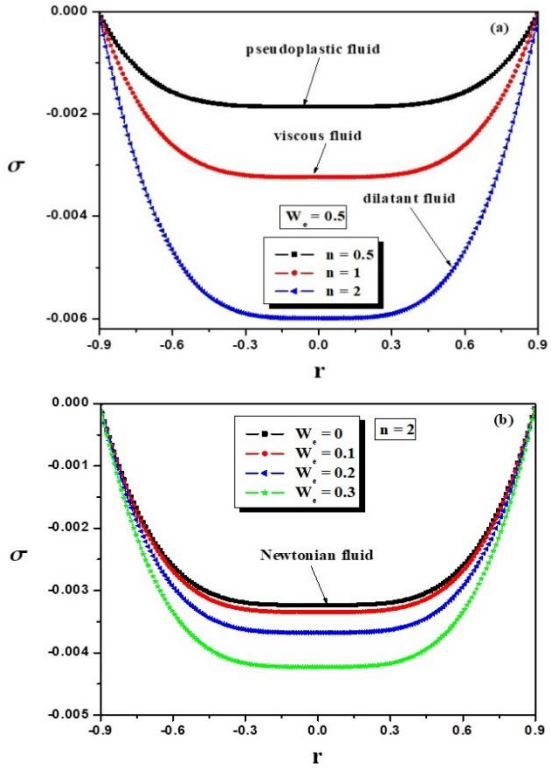

Figure 9. Variation of concentration profiles σ versus r for diversified values of n and W_e at z=1.2, δ^*=0.09, φ=0, q=2, α=15°, F_r=0.1, B_r=0.3, S_r=0.1, S_c=0.1 (panels (a) and (b) respectively)

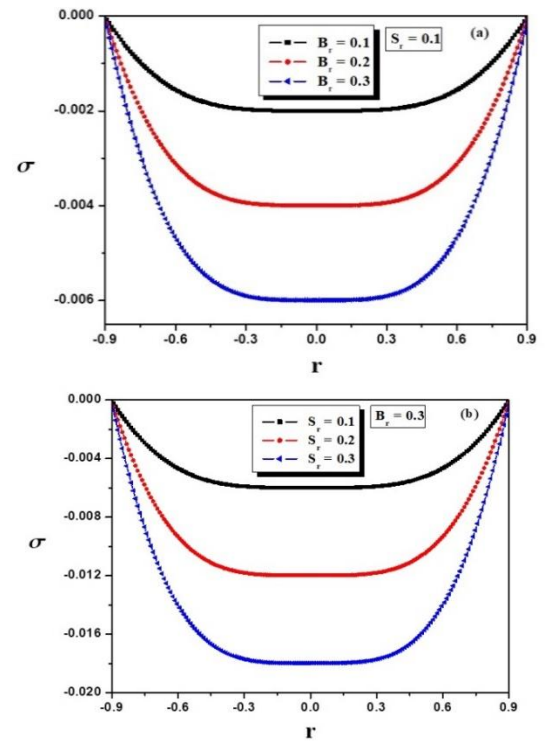

Figure 10. Variation of concentration profiles σ versus r for diversified values of B_r and S_r at z=1.2, δ^*=0.09, φ=0, W_e=0.5, q=2, n=2, α=15°, F_r=0.1, S_c=0.2 (panels (a) and (b) respectively)

The diversity of flow impedance λ with the altitude of the stenosis δ^* for diverse values of the power low index number n, the Weissenberg number W_e, the angle of inclination α and artery length L^* has been shown in Figures 11 and 12. The impedance λ piecemealy enhances as the altitude of the contraction grows. Also impedance curves in the dilatant fluid (n>1) are lower than those in the viscous fluid (n=1) and the pseudoplastic fluid (n<1). Furthermore, the values of resistance for a Newtonian fluid (W_e=0) is higher than that for a Carreau-Yasuda fluid (W_e≠0). Moreover, the impedance along the vertical artery (α=90°) is higher than that along the horizontal artery (α=0°) and the inclined artery (α=30°). It has been perceived from Figure 11(b) that the impedance diminishes with an increment in the Weissenberg number W_e. Also, the impedance grows with enhancement in the artery length L^*, as shown in Figure 12(b).

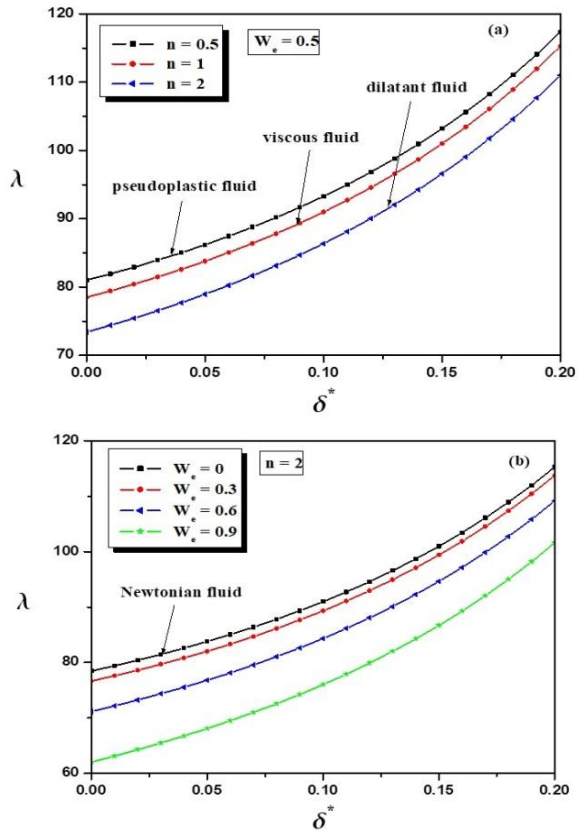

Figure 11. Variance of impedance λ versus δ^* for diversified values of n and W_e at φ=0, q=2, α=60°, F_r=0.1, L^*=3 (panels (a) and (b) respectively)

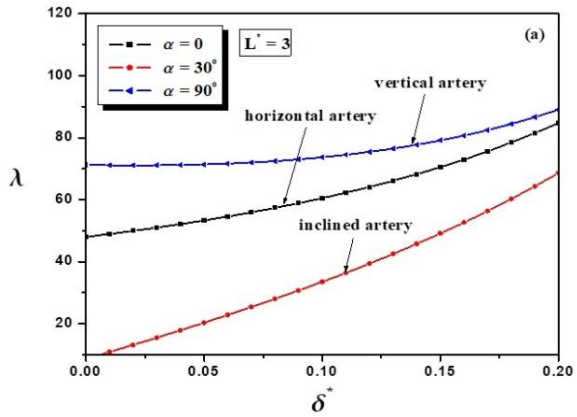

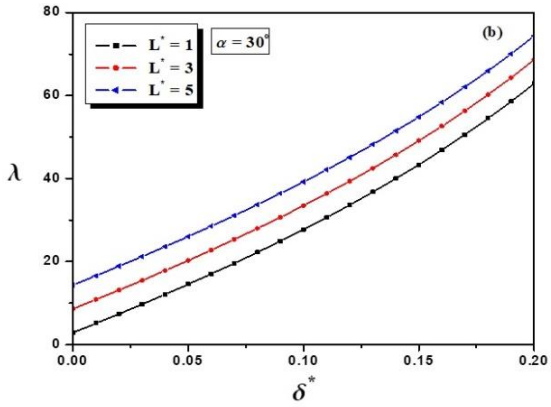

Figure 12. Variance of impedance λ versus δ^* for diversified values of α and L^* at φ=0, W_e=0.3, q=2, n=3, F_r=0.1 (panels (a) and (b) respectively)

The taper angle φ effect is elucidated in Figure 13. It is remarked that the size of the trapping bolus gradually increases, shifting toward the right at (φ=0.2>0) (diverging tapering artery), and it gradually increases moving toward the left at (φ=-0.2<0) (converging tapering artery). Figure 14 depicts the streamlined patterns for diversified values of exponent number n when all other parametric values are kept fixed. It is observed that the streamlines are converging at the upper and lower walls of the artery for the viscous fluid (n=1). It is shown that the streamlines are diverging at the arterial walls noting that there are many circular trapping boluses near the lower border of the artery for the dilatant fluid (n>1). It is seen that the size and the number of the intermittent trapping bolus increase near the lower border of the artery for the pseudoplastic fluid (n<1). Figure 15 indicates that the streamlines are noticeably wider along the vertical artery (α=90°) is maximal than that in the inclined artery (α=30°) and the horizontal one (α=0°).

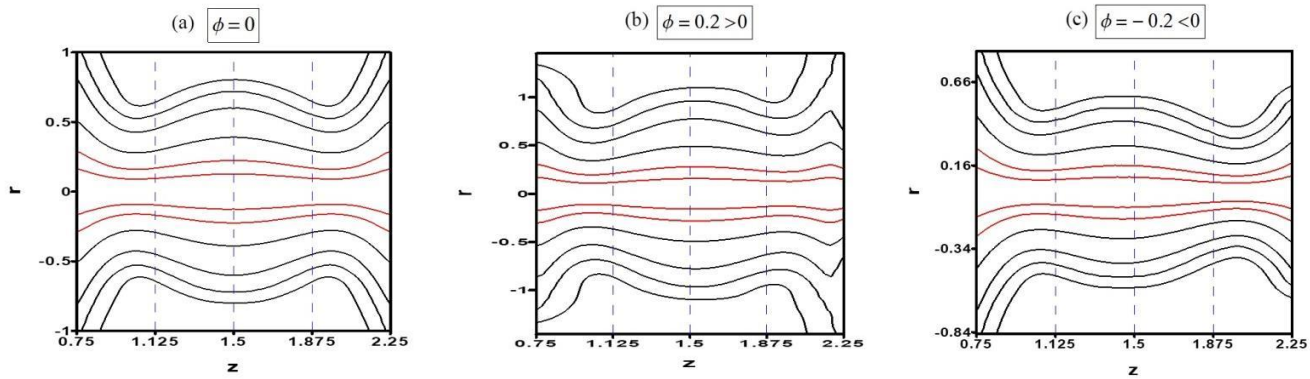

Figure 13. Streamlines for diversified values of the tapering angle φ at δ^*=0.4, W_e=0.3, q=2, n=2, α=45°, F_r=0.1

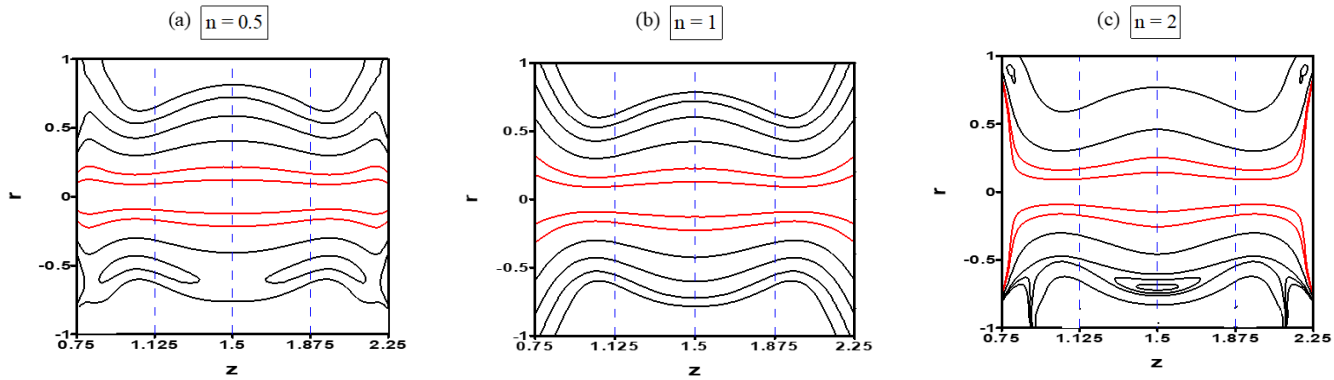

Figure 14. Streamlines for diversified values of the exponent number n at δ^*=0.4, φ=0, W_e=0.5, q=5, α=30°, F_r=0.1

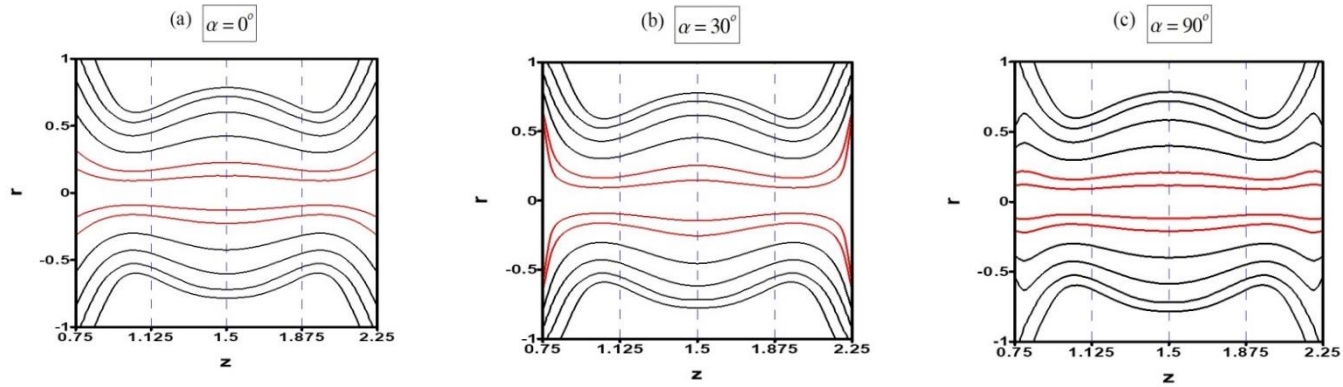

Figure 15. Streamlines for diversified values of tilt angle α at δ^*=0.4, φ=0, W_e=0.5, q=2, n=3, F_r=0.1

5. CONCLUSIONS

An analytical investigation of the flow of a Carreau-Yasuda fluid through the diseased tapered inclined artery subject to heat transfer and chemical reactions has been conducted. The core findings of the analysis are as follows:

●The blood velocity and the temperature curves for the dilatant fluid (n>1) are higher than those in the viscous fluid (n=1) and the pseudoplastic fluid (n<1) in the core region of the artery.

●The values of axial velocity and heat transfer rate along a Newtonian fluid (W_e=0 or n=1) are more minimal than that along a Carreau-Yasuda fluid (W_e≠0 or n≠1) at the core region of the artery.

●The magnitude of blood velocity through the vertical artery is maximal than that in the inclined and horizontal artery inside the core region of the artery.

●The wall shear stress distributions are higher for stenosis (diseased artery) than that for no stenosis (healthy artery).

●The wall shear stress values through the Carreau-Yasuda fluid (W_e≠0 or n≠1) are maximal than that along a Newtonian fluid (W_e=0 or n=1).

●The wall shear stress values along the inclined artery are higher than those in the horizontal and vertical arteries.

●The transmission of the temperature for the Carreau fluid (q=2) is higher than that for the Carreau-Yasuda fluid (q≠2).

●The concentration profile has a reverse behaviour as compared to the temperature profile.

●The impedance gradually increases as the maximum height of stenosis increases.

●The curves of resistance impedance for the dilatant fluid (n>1) are lower than those in the viscous fluid (n=1) and the pseudoplastic fluid (n<1).

●The resistance values for a Newtonian fluid (W_e=0 or n=1) is higher than that for a Carreau-Yasuda fluid (W_e≠0 or n≠1).

●The impedance along the vertical artery is higher than horizontal and inclined arteries.

●The size of the trapping bolus gradually increases, shifting toward the right at (φ>0) (diverging tapering artery), and it gradually increases, moving toward the left at (φ<0) (converging tapering artery).

●The streamlines are noticeably more comprehensive along the vertical artery is higher than that in the inclined artery and the horizontal one.

REFERENCES

[1] Thiriet, M., Delfour, M., Garon, A., Lanzer, P. (2015). Vascular stenosis: An introduction. PanVascular Medicine, pp. 781-868. https://doi.org/10.1007/978-3-642-37078-6_32

[2] Khan, M., Salahuddin, T., Elmasry, Y., Aly, S., Khan, F. (2020). Zero mass flux and convection boundary condition effects on Carreau-Yasuda fluid flow over a heated plat. Radiation Physics and Chemistry, 177: 109152. https://doi.org/10.1016/j.radphyschem.2020.109152

[3] Khan M.I., Alzahrani, F., Hobiny, A., Ali, Z. (2020). Estimation of entropy optimization in Darcy-Forchheimer flow of Carreau-Yasuda fluid (non-Newtonian) with first order velocity slip. Alexandria Engineering Journal, 59(5): 3953-3962. https://doi.org/10.1016/j.aej.2020.06.057

[4] Peralta, J.M., Meza, B.E., Zorrilla, S.E. (2017). Analytical solutions for the free-draining flow of a Carreau-Yasuda fluid on a vertical plate. Chemical Engineering Science, 168: 391-402. https://doi.org/10.1016/j.ces.2017.05.002

[5] Mahmood, R., Bilal, S., Khan, I., Kousar, N., Seikh, A.H., Sherif, E.S.M. (2020). A comprehensive finite element examination of Carreau Yasuda fluid model in a lid driven cavity and channel with obstacle by way of kinetic energy and drag and lift coefficient measurements. Journal of Materials Research and Technology, 9(2): 1785-1800. https://doi.org/10.1016/j.jmrt.2019.12.010

[6] Zaman, A., Ali, N., Sajid, M., Hayat, T. (2015). Effects of unsteadiness and non-Newtonian rheology on blood flow through a tapered time-variant stenotic artery. AIP Advances, 5(3): 037129. https://doi.org/10.1063/1.4916043

[7] Jahangiri, M., Saghafian, M., Sadeghi, M.R. (2017). Numerical simulation of non-Newtonian models effect on hemodynamic factors of pulsatile blood flow in elastic stenosed artery. Journal of Mechanical Science and Technology, 31(2): 1003-1013. https://doi.org/10.1007/s12206-017-0153-x

[8] Samad, A., Husain, A., Zunaid, M., Samad, A. (2017). Newtonian and non-Newtonian pulsatile flows through an artery with stenosis. The Journal of Engineering Research [TJER], 14(2): 191-205. https://doi.org/10.24200/tjer.vol.14iss2pp191-205

[9] Dubey, A., Vasu, B., Bég, O.A., Gorla, R.S.R. (2021). Finite element computation of magneto-hemodynamic flow and heat transfer in a bifurcated artery with saccular aneurysm using the Carreau-Yasuda biorheological model. Microvascular Research, 138: 104221. https://doi.org/10.1016/j.mvr.2021.104221

[10] Liu, H., Lan, L., Abrigo, J., et al. (2021). Comparison of Newtonian and non-Newtonian fluid models in blood flow simulation in patients with intracranial arterial stenosis. Frontiers in Physiology, 12: 718540. https://doi.org/10.3389/fphys.2021.718540

[11] Nazir, U., Abu-Hamdeh, N.H., Nawaz, M., Alharbi, S.O., Khan, W. (2021). Numerical study of thermal and mass enhancement in the flow of Carreau-Yasuda fluid with hybrid nanoparticles. Case Studies in Thermal Engineering, 27: 101256. https://doi.org/10.1016/j.csite.2021.101256

[12] Mekheimer, K.S., Haroun, M.H., El Kot, M.A. (2012). Influence of heat and chemical reactions on blood flow through an anisotropically tapered elastic arteries with overlapping stenosis. Applied Mathematics & Information Sciences, 6(2): 281-292.

[13] Chakravarty, S., Mandal, P. (1996). A nonlinear two-dimensional model of blood flow in an overlapping arterial stenosis subjected to body acceleration. Mathematical and Computer Modelling, 24(1): 43-58. https://doi.org/10.1016/0895-7177(96)00079-9

[14] Mandal, P.K. (2005). An unsteady analysis of non-Newtonian blood flow through tapered arteries with a stenosis. International Journal of Non-Linear Mechanics, 40(1): 151-164. https://doi.org/10.1016/j.ijnonlinmec.2004.07.007

[15] Khan, M.I., Alzahrani, F., Hobiny, A., Ali, Z. (2020). Estimation of entropy generation in Carreau-Yasuda fluid flow using chemical reaction with activation energy. Journal of Materials Research and Technology, 9(5):

9951-9964. https://doi.org/10.1016/j.jmrt.2020.05.085
[16] Nazir, U., Sohail, M., Selim, M. M., Alrabaiah, H., Kumam, P. (2021). Finite element simulations of hybrid nano-Carreau Yasuda fluid with hall and ion slip forces over rotating heated porous cone. Scientific Reports, 11(1): 19064. https://doi.org/10.1038/s41598-021-99116-z
[17] Saha, S., Das, A.N. (2021). Flow bifurcation phenomena of shear-thinning and Newtonian fluids in a rectangular channel in presence of intermediate steps: Using Carreau-Yasuda model. Journal of Applied Fluid Mechanics, 14(4): 1283-1293. https://dx.doi.org/10.47176/jafm.14.04.32136
[18] Hayat, T., Farooq, S., Alsaedi, A., Ahmad, B. (2016). Hall and radial magnetic field effects on radiative peristaltic flow of Carreau-Yasuda fluid in a channel with convective heat and mass transfer. Journal of Magnetism and Magnetic Materials, 412: 207-216. https://doi.org/10.1016/j.jmmm.2016.03.046
[19] Hayat, T., Abbasi, F.M., Ahmad, B., Alsaedi, A. (2014). Peristaltic transport of Carreau-Yasuda fluid in a curved channel with slip effects. PloS One, 9(4): e95070. https://doi.org/10.1371/journal.pone.0095070
[20] Khan, M.I., Hayat, T., Afzal, S., Khan, M.I., Alsaedi, A. (2020). Theoretical and numerical investigation of Carreau-Yasuda fluid flow subject to Soret and Dufour effects. Computer Methods and Programs in Biomedicine, 186: 105145. https://doi.org/10.1016/j.cmpb.2019.105145
[21] Kefayati, G.R., Tang, H. (2019). Three-dimensional Lattice Boltzmann simulation on thermosolutal convection and entropy generation of Carreau-Yasuda fluids. International Journal of Heat and Mass Transfer, 131: 346-364. https://doi.org/10.1016/j.ijheatmasstransfer.2018.11.076
[22] Young, D.F. (1968). Effect of a time dependent stenosis of flow through a tube. Journal of Engineering and Industrial, 90(2): 248-254. https://doi.org/10.1115/1.3604621
[23] Padma, R., Selvi, R.T., Ponalagusamy, R. (2021). Analysis of MHD pulsatile flow of Jeffrey fluid in a diseased inclined tapered porous artery exposed to an inclined magnetic field. Journal of Physics: Conference Series, 1850(1): 012039. https://doi.org/10.1088/1742-6596/1850/1/012039
[24] Farooq, M., Rahim, M.T., Islam, S., Siddiqui, A.M. (2013). Steady Poiseuille flow and heat transfer of couple stress fluids between two parallel inclined plates with variable viscosity. Journal of the Association of Arab Universities for Basic and Applied Sciences, 14(1): 9-18. http://dx.doi.org/10.1016/j.jaubas.2013.01.004
[25] Alam, N., Poddar, S., Karim, M.E., Hasan, M.S., Lorenzini, G. (2021). Transient MHD radiative fluid flow over an inclined porous plate with thermal and mass diffusion: An EFDM numerical approach. Mathematical Modelling of Engineering Problems, 8(5): 739-749. https://doi.org/10.18280/mmep.080508

NOMENCLATURE

B_r	Brickmann number
C	concentration, Kg. m^{-2} .s^{-2}
c_p	specific heat capacity, J. Kg^{-1}. K^{-1}
C_0 & C_1	walls concentration, Kg. m^{-2} .s^{-2}
D	diffusion coefficient, m^2. s^{-1}
d	site of the stenosis, m
d^*	dimensional stenosis site
dp_0/dz	initial pressure rise, Kg. m^{-2}. s^{-2}
F	flow rate, m^3.s^{-1}
F_r	Froud number
G	gravitational acceleration, m. s^{-2}
K	thermal conductivity, W. m^{-1}. K^{-1}
K_T	thermal-diffusion ratio, Kg. m^{-2} .s^{-2}
$3L_0/2$	length of overlapping stenosis, m
L^*	non-dimensional length of arterial segment
m^*	slope of the tapered vessel
n	power low index number
p	pressure, N. m^{-2}
P_r	Prandtl number
q	Carreau-Yasuda parameter
R	radius of the tapered artery, m
r	radial direction, m
R_e	Reynolds number
R_0	radius of the non-tapered artery, m
S_c	Schmidt number
S_r	Soret number
T	temperature field, K
t	time, s
T_m	temperature of the medium, K
T_0 & T_1	walls temperature, K
u_0	average velocity of the fluid over arterial segment, m. s^{-1}
V_z	axial velocity, m. s^{-1}
V_r	radial velocity, m. s^{-1}
W_e	Weissenberg number
z	axial direction, m

Greek symbols

α	angle of inclination
δ	height of the stenosis, m
δ^*	dimensionless height of the stenosis
θ	dimensionless temperature
λ	resistance impedance, Kg. m^{-4}. s^{-1}
μ_0 & μ_∞	viscosity at zero and infinite shear rates, Kg. m^{-1}. s^{-1}
ρ	fluid density, Kg. m^{-3}
σ	dimensionless concentration
τ_R	wall shear stress distribution, N. m^{-2}
ϕ	angle of tapering
ψ	stream function, m^3. s^{-1}
Γ	time constant
Δp	pressure drop, Kg. m^{-1}. s^{-2}